Ultrasensitive, stretchable, and transparent humidity sensor based on ion-conductive double-network hydrogel thin films

Zixuan Wu[1†], Qiongling Ding[1†], Zhenyi Li[1†], Zijing Zhou[1], Luqi Luo[1], Kai Tao[2], Xi Xie[1] and Jin Wu[1*]

ABSTRACT   Ion-conductive hydrogels with intrinsic biocompatibility, stretchability, and stimuli-responsive capability have attracted considerable attention because of their extensive application potential in wearable sensing devices. The miniaturization and integration of hydrogel-based devices are currently expected to achieve breakthroughs in device performance and promote their practical application. However, currently, hydrogel film is rarely reported because it can be easily wrinkled, torn, and dehydrated, which severely hinders its development in microelectronics. Herein, thin, stretchable, and transparent ion-conductive double-network hydrogel films with controllable thickness are integrated with stretchable elastomer substrates, which show good environmental stability and ultrahigh sensitivity to humidity (78,785.5%/% relative humidity (RH)). Benefiting from the ultrahigh surface-area-to-volume ratio, abundant active sites, and short diffusion distance, the hydrogel film humidity sensor exhibits 2×10^5 times increased response to 98% RH, as well as 5.9 and 7.6 times accelerated response and recovery speeds compared with the bulk counterpart, indicating its remarkable thickness-dependent humidity-sensing properties. The humidity-sensing mechanism reveals that the adsorption of water improves the ion migration and dielectric constant, as well as establishes the electrical double layer. Furthermore, the noncontact human-machine interaction and real-time respiratory frequency detection are enabled by the sensors. This work provides an innovative strategy to achieve further breakthroughs in device performance and promote the development of hydrogel-based miniaturized and integrated electronics.

Keywords: stretchable hydrogel, humidity sensor, thin-film, ultrasensitive, wearable application

INTRODUCTION

Conductive hydrogels featured with the effective integration of mechanical stretchability and conductivity, are currently one of the most widely investigated materials in flexible and stretchable electronics and have shown considerable application potential in wearable/portable electronics, energy storage devices, artificial intelligence, biomedicine, and other fields [1–6]. Particularly, hydrogels can be exploited to prepare various sensors to detect strain/pressure, temperature, humidity, and gas by converting these external stimuli into detectable electrical signals (resistance or capacitance variations) [7–16]. Despite their intriguing stretchability, flexibility, and transparency in fabricating wearable electronics, the mechanical properties, miniaturization, and stability of hydrogel-based devices still demand improvement for practical applications. To this end, considerable effort has been devoted to improving and optimizing the electromechanical properties and functionalities of hydrogels, such as introducing multiple networks, adding nanofillers, and modifying functional groups [17,18]. Equally important is the miniaturization of hydrogels, which is necessary for the development of miniature smart electronics in the future. Thus, the preparation of stable and stretchable hydrogel thin films with minimum thickness for developing high-performance and miniaturized devices is imperative. However, some challenges severely hinder the development of hydrogel films. First, the crosslinking at the interface of the hydrogel is usually poor, and the resulting micrometer-scale defects on the surface cause the mechanical properties of the hydrogel film to deteriorate sharply as the thickness of the hydrogel decreases [19]. Moreover, the hydrogel will inevitably be gradually dehydrated in ambient air and frozen at low temperatures, leading to the deterioration of both material shape and various properties, which becomes more serious after the thickness decreases because of the large contact area with the surrounding environment. Even for humidity-sensing applications, the inevitable dehydration of hydrogels limits the detection range [20–22].

Humidity detection has practical significance in our lives. For example, human skin is a typical humidity source; therefore, the high-precision detection of the humidity field around it can be expected to realize a noncontact human-machine control system, which helps solve the inevitable abrasion, pollution, and virus transmission problems caused by traditional contact sensing [23]. Moreover, the humidity of the exhaled air is closely related to human health; thus, the development of high-precision humidity sensors can play an important role in the real-time monitoring of human health [24]. Particularly, the monitoring of human respiration is useful and convenient for evaluating the health condition of patients in the current global COVID-19 pandemic [25]. Currently, various humidity sensors based on graphene and its derivatives [26–36], metal oxides or sulfides [37–43], and conducting polymers [44,45] have been developed based on the changes in the electrical properties (i.e.,

[1] State Key Laboratory of Optoelectronic Materials and Technologies and the Guangdong Province Key Laboratory of Display Material and Technology, School of Electronics and Information Technology, Sun Yat-sen University, Guangzhou 510275, China
[2] The Ministry of Education Key Laboratory of Micro and Nano Systems for Aerospace, Northwestern Polytechnical University, Xi'an 710072, China
† These authors contributed equally to this work.
* Corresponding author (email: wujin8@mail.sysu.edu.cn)

capacitance, resistance, and impedance) or weight of these materials after adsorbing water molecules [37,46–48]. Nevertheless, most humidity sensors have suboptimal sensing performance and lack flexibility. To address this problem, more hierarchically structured nanomaterials with high specific surface areas are designed to produce a high humidity response, and flexible substrates are always utilized. For example, Lan *et al.* [28] used laser direct writing technology to induce the formation of graphene oxide on flexible interdigital electrodes, and the resulting flexible humidity sensor exhibited a low hysteresis, high sensitivity, and excellent stability of <1% response variation within one year. Notably, this sensor can be directly attached to plant leaves for the detection of subtle relative humidity (RH) changes caused by plant leaf transpiration. Zhang *et al.* [37] used self-assembly technology to prepare a flexible humidity sensor based on tin disulfide nanoflowers and zinc stannate hybrid thin-film. The large specific surface area of tin disulfide nanoflowers accelerates the adsorption and desorption processes of water molecules on the surface of the film. The hollow nanosphere structure of zinc stannate also has a large surface area and facilitates the contact and charge transfer of water molecules. Although limited flexibility is achieved, the lack of stretchability of these sensing materials limits their further development in stretchable and wearable electronic applications. Therefore, the development of stretchable humidity sensors using intrinsically stretchable materials is highly desired.

Notably, the water-rich hydrogel exhibits good sensitivity to water molecules in the environment and can electrically respond to external changes in RH because of the rapid adsorption and desorption of water molecules. More importantly, the stretchability of the hydrogel can be easily improved by introducing more non-covalent interactions to the network to effectively dissipate energy, resulting in a humidity sensor with better stretchability. For example, Wu *et al.* [7] exploited a one-step polymerization method to prepare a polyacrylamide (PAM)/carrageenan double-network (DN) hydrogel, and on this basis, a stretchable, transparent, and self-repairing humidity sensor was recently prepared. Although some hydrogel-based humidity sensors have been reported, their responsiveness has not been improved, and the growing demands of practical application are difficult to meet [7,49,50]. This problem can be attributed to the low surface-area-to-volume ratio of the current bulk hydrogel material and the limited diffusion of external stimuli inside the hydrogel, and the exploration of some strategies that can considerably improve the sensitivity of the hydrogel-based humidity sensor is highly desired. Thus, the construction of hydrogel films can significantly enhance the responsiveness of hydrogels to humidity because of the ultrahigh surface-area-to-volume ratio and abundant active sites. Taking into account the advantages of the hydrogel film structure, for example, a 150-μm-thick hydrogel film is used as the electrolyte of a wearable electrochemical biosensor to achieve the measurement of transcutaneous oxygen pressure; this ultrathin porous structure of the hydrogel film is conducive to the rapid penetration of oxygen molecules diffused from the skin surface [51]. Moreover, the reduction of the thickness of the hydrogel will correspondingly lead to an increase in light transmittance, which can considerably broaden its application in fields with high optical requirements [52]. Notably, detailed quantitative studies of the influence of the thickness of the hydrogel on the humidity-sensing performance are still lacking [7]. Overall, the develop-

ment of stretchable hydrogel thin films may provide a new perspective for the design of miniaturized electronic devices with high sensing performance. However, research on hydrogel thin-film-based humidity sensors is rare. Furthermore, more in-depth exploration and research on their sensing mechanism are required [53,54].

Inspired by these observations, in this study, PAM/carrageenan hydrogel thin films were successfully integrated with the plasma-treated elastomeric polydimethylsiloxane (PDMS) substrate for the preparation of intrinsically stretchable, transparent, and high-performance thin-film humidity sensors for the first time (Scheme 1). The thicknesses of hydrogel films can be readily tuned by adjusting the speed of spin-coating, and the minimum thickness reached 6.06 μm. By immersing the hydrogels in a lithium bromide (LiBr) solution, their drying and frost resistances were enhanced (Fig. 1). The influences of LiBr concentration, working frequency, and film thickness on the sensor performance were systematically explored. For the 6.06-μm-thick hydrogel film, its capacitance changed by up to 5,500,000% as the RH increased from 11% to 98%, and its sensitivity reached as high as 78,785.5%/% RH (Scheme 1c), indicating 2×10^5 times increased response to 98% RH compared with the bulk counterpart. Moreover, the thin-film sensor exhibited a short response/recovery time (i.e., 201 and 41 s) and good repeatability (0.4% error for four cycles), which indicates 5.9 and 7.6 times accelerated response and recovery speeds compared with the bulk counterpart, respectively, showing the remarkably boosted sensing performance compared with that reported in previous studies. Through complex impedance spectroscopy, the adsorption behavior and internal electrical changes of the hydrogel film under different RH ranges and the sensing mechanism were analyzed in depth. More impressively, compared with the ultrahigh response to humidity, this sensor was nearly insensitive to temperature and pressure, indicating excellent selectivity. As a consequence, this ultrasensitive humidity sensor could realize noncontact detection of humidity around human skin, and the response changed accordingly as the finger gradually moved away from the sensor. Meanwhile, this ultrasensitive humidity sensor could be utilized to detect the subtle RH changes caused by human breathing under different frequencies. The intriguing performance and practical applications reveal the potential of this stretchable hydrogel film humidity sensor for wearable applications.

EXPERIMENTAL SECTION

Preparation of PAM/carrageenan DN hydrogel precursor solution
A hydrogel precursor solution was produced by mixing acrylamide (7.5 g), carrageenan (1.5 g), *N,N*-methylene-bis-acrylamide (5 mg), chloride (KCl; 90 mg), photoinitiator (Irgacure 2959; 100 mg), and deionized water (41 mL) in a flask. After stirring at 95°C in an oil bath for 5 h, each component was dispersed uniformly.

Preparation of the bulk hydrogel
The as-prepared hydrogel precursor was poured into a glass petri dish with a diameter of 60 mm. Then, the petri dish was placed in a refrigerator at 6°C for 1 h. After refrigeration, the first network of κ-type carrageenan was formed. Then, an ultraviolet (UV) lamp was deployed to irradiate the sample for 2 h to induce the polymerization of acrylamide. Finally, the
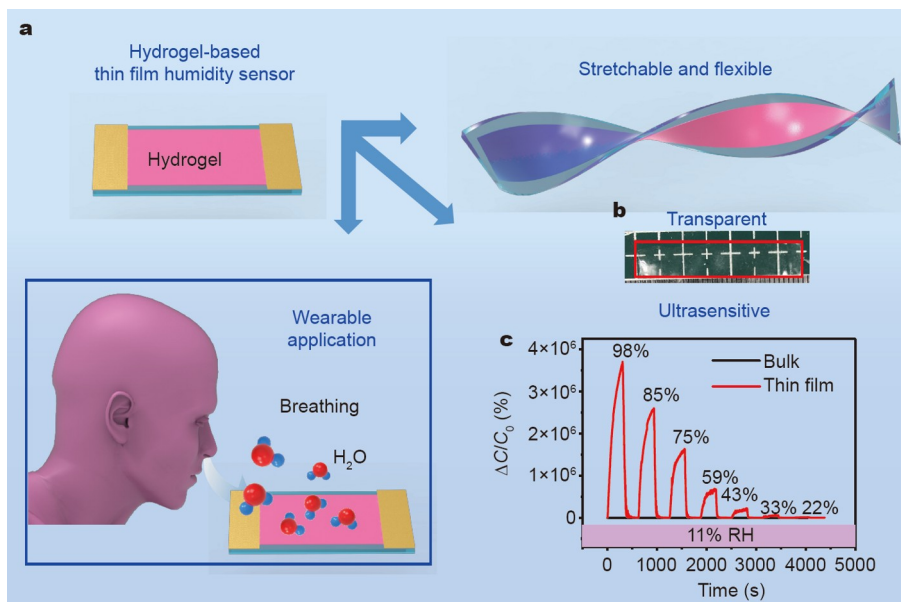
Scheme 1 (a) Schematic of the hydrogel film humidity sensor with high deformability and its practical application in respiration monitoring. (b) Photograph showing the hydrogel film with excellent transparency, as denoted by the white marks beneath the film. (c) Dynamic capacitance responses of bulk and thin-film hydrogel sensors under different RH ranges indicate the ultrahigh sensitivity of the film sensors.
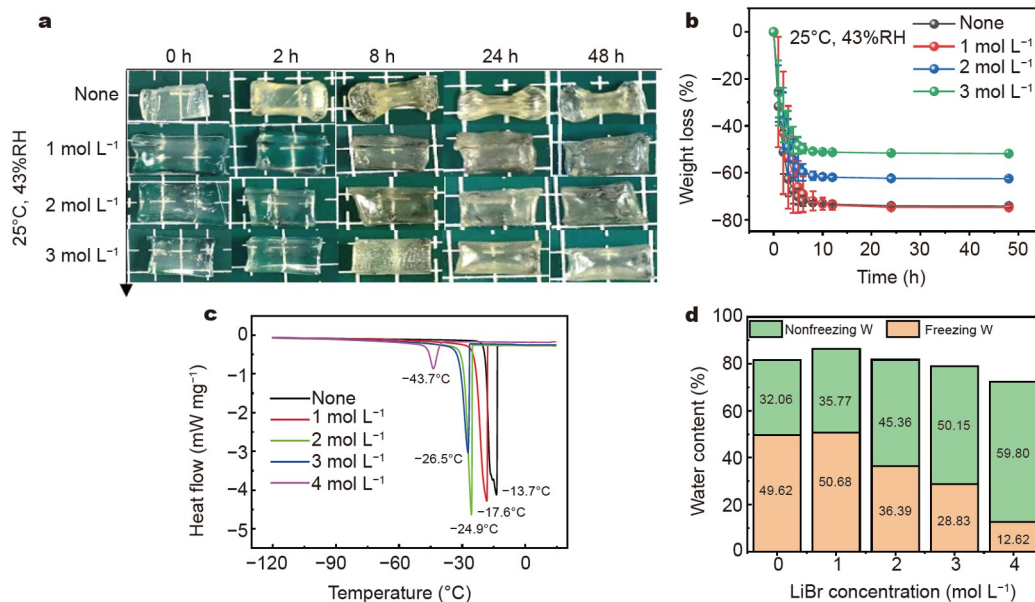

Figure 1 Effects of LiBr on the anti-drying and anti-freezing capabilities of the hydrogel. (a) Morphology evolution of the original hydrogel (none) and LiBr-percolated hydrogels with different LiBr concentrations when placed in a dry environment at 25°C and 43% RH for 0–48 h. (b) Curves of the weight losses of these hydrogels during the course. (c) DSC spectra of these hydrogels. (d) Proportions of freezing and nonfreezing water in these hydrogels.

original hydrogel with a DN structure was formed. For comparison, the original hydrogel was cut into 1 cm × 0.5 cm bulk hydrogels, which were then immersed in LiBr solution with different concentrations (1–4 mol L^{-1}) for 2 h to prepare bulk hydrogels with different LiBr contents for the investigation of their properties.

Preparation of the thin-film hydrogel

The preparation process of PAM/carrageenan hydrogel film is shown in Fig. 2b (right). The PDMS precursor was prepared by

mixing Dow Corning 184 and the corresponding curing agent with the ratio of 10:1 in a plastic cup. Then, the prepolymer was homogenized in a rotating and revolving mixer for 60 s. A heat-resistant tape was wrapped around the 3 cm × 3 cm aluminum (Al) sheet, which facilitates the peeling off of the film sensor after the preparation of the hydrogel film. Approximately 2 g of PDMS prepolymer was spin-coated onto the Al sheet at a rotation speed of 1000 r min^{-1} for 30 s. Subsequently, the Al sheet was placed on a hot plate at 80°C to cure PDMS for 2 h. Before spin-coating the hydrogel precursor onto the PDMS-
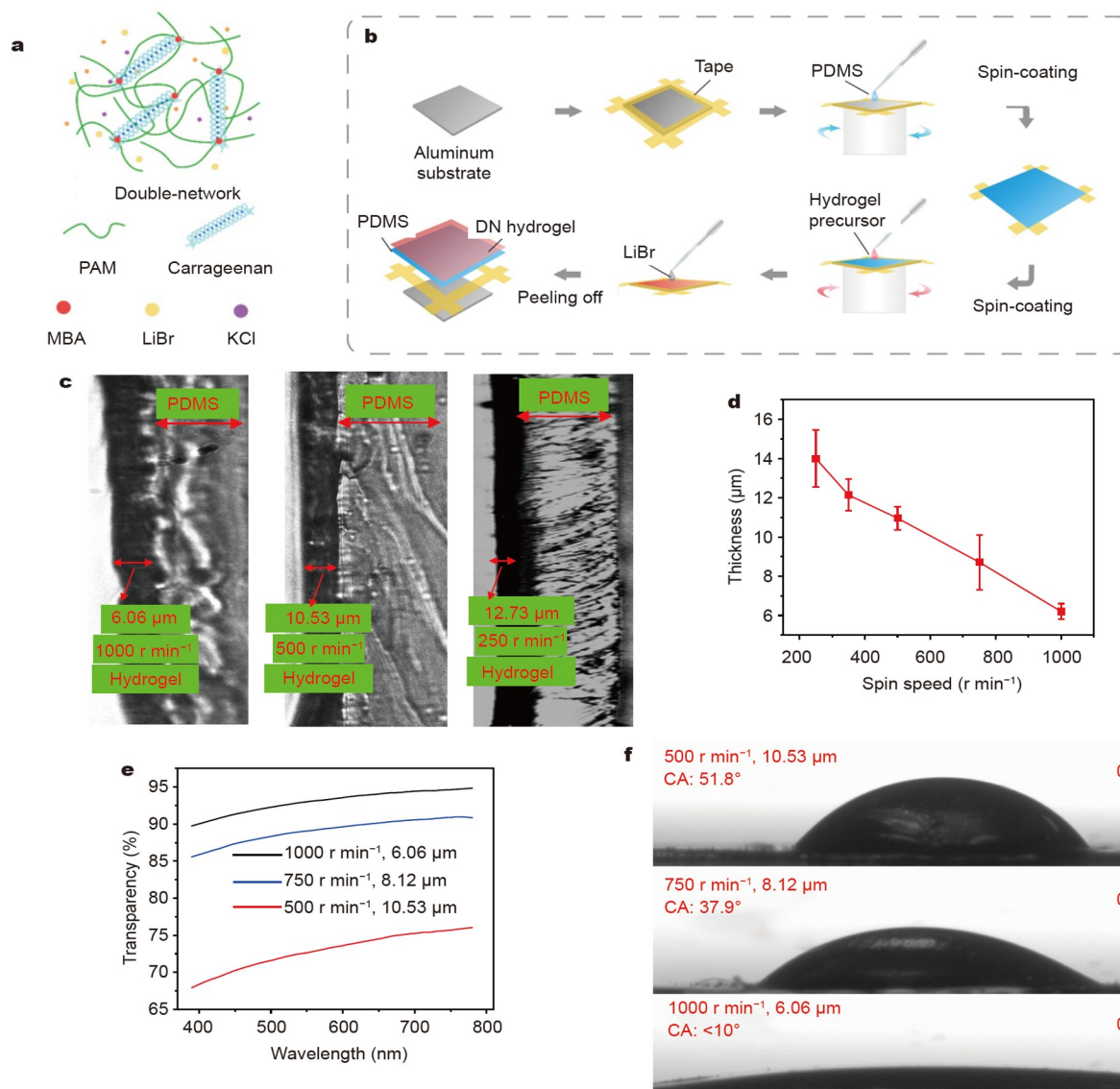
Figure 2 (a) Schematic illustrating the structure of LiBr-PAM/carrageenan DN hydrogel. (b) Scheme showing the fabrication process of the hydrogel thin-film-based humidity sensor *via* a layer-by-layer spin-coating technology. (c) Photographs showing the cross-sectional profiles of the thin-film sensors fabricated using the spin-coating speeds of 1000, 500, and 250 r min^{-1}, generating hydrogel layers with thicknesses of 6.06, 10.53, and 12.73 μm, respectively. (d) Curves of the thickness changes of the hydrogel film with the spin-coating speed. (e) Visible light transmittance of the sensors fabricated with the spin-coating speed of 500–1000 r min^{-1}. (f) The contact angles of water on the 1 mol L^{-1} LiBr-percolated hydrogel films with thicknesses of 6.06, 8.12, and 10.53 μm are <10.0°, 37.9°, and 51.8°, respectively.

coated Al sheet substrate, the PDMS substrate was treated with oxygen plasma for 5 min (120 W) to render it hydrophilic. Afterward, hydrogel films with different thicknesses were obtained by spin-coating 5 mL of the hydrogel precursor onto the PDMS substrate under different speeds for 30 s and polymerizing them in the same manner as bulk hydrogels (cooled at 6°C for 1 h and UV irradiation for 2 h). The difference is that, before UV irradiation, to effectively prevent the rapid dehydration of the hydrogel precursor solution because of the excessively high temperature of the UV lamp, 2 mL of LiBr solution with different concentrations was dropped on the surface of the sample, which could promote the crosslinking of the hydrogel. After the photopolymerization was completed, the LiBr solution was poured out, and the residual solution on the surface of the hydrogel film was absorbed by a filter paper.

Material characterization

The UV-visible (vis) spectra were recorded using a UV-vis spectrophotometer (Thermo Fisher, Inc. Evolution 220) with a wavelength of 390–780 nm. The differential scanning calorimetry (DSC) spectra were recorded using a differential scanning calorimeter (Netzsch, DSC-204 F1) at a cooling rate of 5°C min^{-1} from 25 to −120°C with nitrogen flow. The strain-stress curves were obtained using an Instron machine (S6566). The contact angles were acquired at the moment when a water droplet (5 μL of deionized water) was dropped on the surface of hydrogel films using a contact angle measurement instrument (Beijing Audelino Instrument Co., Ltd. OCA15EC).

Humidity-sensing measurement

The hydrogel film was cut into a sheet with the size of 1 cm ×

0.5 cm to measure the resistance and capacitance using an LCR meter (Tonghui, TH2832, 200 Hz–200 kHz). Different RH ranges were obtained using bottles containing different saturated salt solutions. Specifically, saturated potassium sulfate (K_2SO_4), KCl, sodium chloride (NaCl), sodium bromide (NaBr), potassium carbonate (K_2CO_3), magnesium chloride ($MgCl_2$), potassium acetate (CH_3COOK), and lithium chloride (LiCl) solutions provided 98%, 85%, 75%, 59%, 43%, 33%, 22%, and 11% RH, respectively (calibrated by a digital thermo-hygrometer (CEM, SA615)). For the detection of RH in each cycle, the hydrogel film was placed in the bottle with 11% RH for signal stabilization, moved to another bottle with a different RH to respond for 300 s, and moved back to the original bottle for 300 s for signal recovery (Fig. S1). The response time of the experiment was set as 600 s to evaluate repeatability.

RESULTS AND DISCUSSION

The easy drying and freezing of hydrogels considerably limit their service life and usable environment, which are some of the most important concerns for their practical application as sensors. Here the incorporation of LiBr in the hydrogel significantly inhibits its tendency to both dehydrate and freeze. As shown in Fig. 1a, the morphologies of the original hydrogel (none) and bulk hydrogels immersed in 1–3 mol L^{-1} LiBr solution after being placed in a dry environment of 25°C and 43% RH for different periods were recorded. Results show that the original hydrogel loses water at high speed, and its volume decreases significantly after being left for 8 h. Thus, the hydrogel becomes fragile after 48 h. By contrast, even after being left for 48 h, the morphologies and volumes of the hydrogels immersed in 1–3 mol L^{-1} LiBr solution did not decrease significantly, and only a small amount of water was lost. The mass loss percentages of the hydrogels immersed in 1, 2, and 3 mol L^{-1} LiBr solutions after 48 h are 74%, 62%, and 52%, respectively (Fig. 1b), which proves that the anti-drying capability of the hydrogel is gradually improved as the LiBr concentration increases. This finding indicates the important role of LiBr in enhancing the moisture-holding capability of the hydrogel. The hydrogel film without LiBr percolation easily dries out and is fragile. The introduction of LiBr prevents the cracking and failure of the thin-film sensor. Furthermore, compared with the bulk hydrogel, the thin-film hydrogel absorbs a higher proportion of water and LiBr during immersion for 2 h. The calculated weight ratio of LiBr in the thin-film hydrogel is 6.6%, which is 2.27 times higher than that in bulk hydrogel and close to that in 1 mol L^{-1} LiBr solution (~8%), indicating the higher immersion efficiency of the hydrogel thin film (Fig. S2 and Table S1). Meanwhile, the weight change of the film after being stored under different RH ranges for 12 h is shown in Fig. S3. The thin-film sensor (1 mol L^{-1} LiBr) losses 20% weight of water after being stored at 25°C, 43% RH for 12 h. However, the thin-film sensor absorbs water from the air, which increases its weight to 91% of the initial state after being stored at 25°C, 67% RH for 12 h. Notably, part of the hydrogel is a small fraction of the mass of the film sensor because of the PDMS substrate, indicating its high water exchange efficiency with the environment, which is beneficial to highly sensitive humidity detection.

Moreover, reducing the freezing point of the hydrogel is of significance for its stable operation at a low temperature, and the introduced LiBr can effectively inhibit the formation of ice crystals in the hydrogel. The DSC curves (Fig. 1c) show that the freezing point of the original bulk hydrogel is −13.7°C, whereas those of the bulk hydrogels after being immersed in 1, 2, 3, and 4 mol L^{-1} LiBr solutions are −17.6, −24.9 , −26.5 , and −43.7°C, respectively, showing gradually enhanced anti-freezing capability as the LiBr concentration increases. The hydrogel thin-film sensor (1 mol L^{-1} LiBr) maintains high flexibility after being stored at 0°C for 12 h (Fig. S4). Generally, ice is an infinite network of hydrogen bonds formed between water molecules [55]. In this case, after the introduction of LiBr, lithium and bromide ions can polarize with water molecules to form hydrates, which are difficult to freeze at low temperatures, generating the ice formation inhibition effects of LiBr. Quantitatively, as shown in Fig. 1d, the total moisture content of the original hydrogel is 81.68%, which specifically contains 32.06% nonfreezing water and 49.62% freezing water. For the LiBr-incorporated hydrogels, the proportion of internal nonfreezing water gradually increases from 32.06% to 59.80% as the LiBr concentration increases from 0 to 4 mol L^{-1} LiBr, and the proportion of freezing water gradually decreases from 49.62% to 12.62% accordingly [56]. This finding confirms the conversion of free water to nonfreezing water after the introduction of LiBr. Consequently, enhanced frost resistance is exhibited in the hydrogel.

In the past, research on hydrogel-based humidity sensors mainly focused on the exploration and modification of materials, leaving the significant impact of the structure and size of the hydrogel on the sensing performance unexplored [49,50,57–61]. Here, the humidity-sensing performance is enhanced, and the device is miniaturized by utilizing hydrogel thin film as the transducing material. As shown in Fig. 2a, b, the LiBr-incorporated PAM/carrageenan hydrogel thin films with controllable thickness were fabricated on a PDMS thin film using the spin-coating process with different speeds, which is described in detail in the "EXPERIMENTAL SECTION". More importantly, we percolated LiBr into the hydrogel to prevent the dehydration of the hydrogel during the polymerization process. Furthermore, we wrapped the edges of the thin film with heat-resistant tape to promote the peeling off of the as-fabricated thin film from the Al substrate (Fig. 2b). To analyze the influence of spin-coating speed on the thickness of hydrogel films, the cross-sectional profiles of the hydrogel films prepared under different spin-coating speeds are obtained under the same RH, as shown in Fig. 2c. With the increase in spin-coating speed, the thickness of the hydrogel film gradually decreases. Specifically, hydrogel films with thicknesses of 14.03 ± 1.46, 12.14 ± 0.81, 10.96 ± 0.59, 8.72 ± 1.40, and 6.20 ± 0.40 μm were prepared using the spin-coating speeds of 250, 350, 500, 750, and 1000 r min^{-1}, respectively (Fig. 2d). Meanwhile, the thickness has a significant impact on the transparency of hydrogel films. For the 10.53-μm-thick hydrogel film, the visible light (390–780 nm wavelength) transparency is between 67.9% and 76.0%, which increases to between 85.6% and 90.8% and between 89.8% and 94.8% when the thickness is reduced to 8.12 and 6.06 μm, respectively (Fig. 2e). This increase can be mainly attributed to less interference with visible light after the thickness is reduced, leading to the visualization of the underlying substrate without impeding the function of the sensor. Moreover, the hydrophilicity of the hydrogel is another important parameter for humidity-sensing applications, which correlates with the thickness of the hydrogel film. As shown in Fig. 2f, the contact angles of water on the hydrogel films with thicknesses of 10.53, 8.12, and 6.06 μm are

51.8°, 37.9°, and <10.0°, respectively, which are all <90°, indicating that the surface of hydrogel films is hydrophilic. Furthermore, the contact angle decreases remarkably as the thickness of the hydrogel film decreases. This finding can be attributed to the reduction of the difference in surface tension between the hydrogel film and the water droplets, resulting in a more hydrophilic surface [62]. Correspondingly, water molecules can be easily adsorbed on the surface of the hydrogel film, leading to high sensitivity in humidity sensing.

Subsequently, the dynamic capacitance variations of the humidity sensors based on bulk and thin-film hydrogels in response to RH ranging from 98% to 22% were compared, as shown in Fig. 3a and Fig. S5. The thin-film humidity sensor exhibits a reversible and rapid response process, indicating the rapid adsorption and desorption of water molecules on the hydrogel film. For a better comparison of sensitivity, the real-time capacitance response curves of the two sensors were combined and compared, as shown in Fig. 3b. The capacitance response ($\Delta C/C_0$) here is defined as the capacitance change relative to the initial capacitance C_0 (the capacitance at 11% RH). Under the same humidity, the response of the thin-film humidity sensor is several orders of magnitude higher than that of the bulk counterpart, indicating that the construction of the hydrogel thin film has led to a significant increase in sensitivity. Ideally, bulk and thin-film hydrogels can be regarded as rectangular parallelepipeds with the same length and width (1 cm × 0.5 cm) but different thicknesses. Without considering the porous structure and vapor diffusion in the hydrogel, their surface-area-to-volume ratio can be simply defined as the external surface area of the hydrogel divided by the volume. Consequently, the surface-area-to-volume ratio of the bulk hydrogel with a thickness of 0.5 cm is calculated to be only $1 \times 10^{-3} \, \mu m^{-1}$,

whereas that of the hydrogel film with a thickness of 6.06 μm is as high as $1.67 \times 10^{-1} \, \mu m^{-1}$, indicating an increment of 167 times. Furthermore, it is more difficult for the adsorbed water molecules to diffuse into the inner part of bulk hydrogel, leading to longer diffusion distance for both adsorption and desorption of water molecules in comparison with the thin-film hydrogel. Beyond that, the initial capacitances C_0 of the bulk and thin-film humidity sensors are of the orders of 10^{-6} and 10^{-11} F, respectively. Because the initial capacitance C_0 of the thin-film humidity sensor is five orders of magnitude lower than that of the bulk counterpart, the same amount of capacitance variation ΔC caused by the humidity change leads to the increased response of the thin-film humidity sensors.

To further systematically investigate the influence of the thickness of the hydrogel film on the humidity-sensing properties, the responses of the humidity sensors based on different thicknesses of hydrogel film are plotted as a function of RH (from 11% to 98%), as shown in Fig. 3c. Among the four thickness levels, the thinnest hydrogel film prepared at 1000 r min^{-1} exhibits the highest capacitance responses of 1262% and 5,500,000% to 22% and 98% RH, respectively. By contrast, the bulk hydrogel sensor exhibits the lowest capacitance responses of 0.68% and 27% to 22% and 98% RH, respectively. For the other two hydrogel films prepared at 500 and 750 r min^{-1}, their capacitance responses to 98% RH are also up to 175,000% and 627,400%, respectively, which are lower than that of the thinnest hydrogel film but far exceed that of bulk hydrogels. Hence, the sensitivity of the hydrogel to humidity increases sharply as its thickness decreases. Particularly, at low humidity, the capacitance response of the 6.06-μm-thick hydrogel film sensor is 1855 times that of the bulk counterpart, and at high humidity, it increases to as high as 203,703 times.
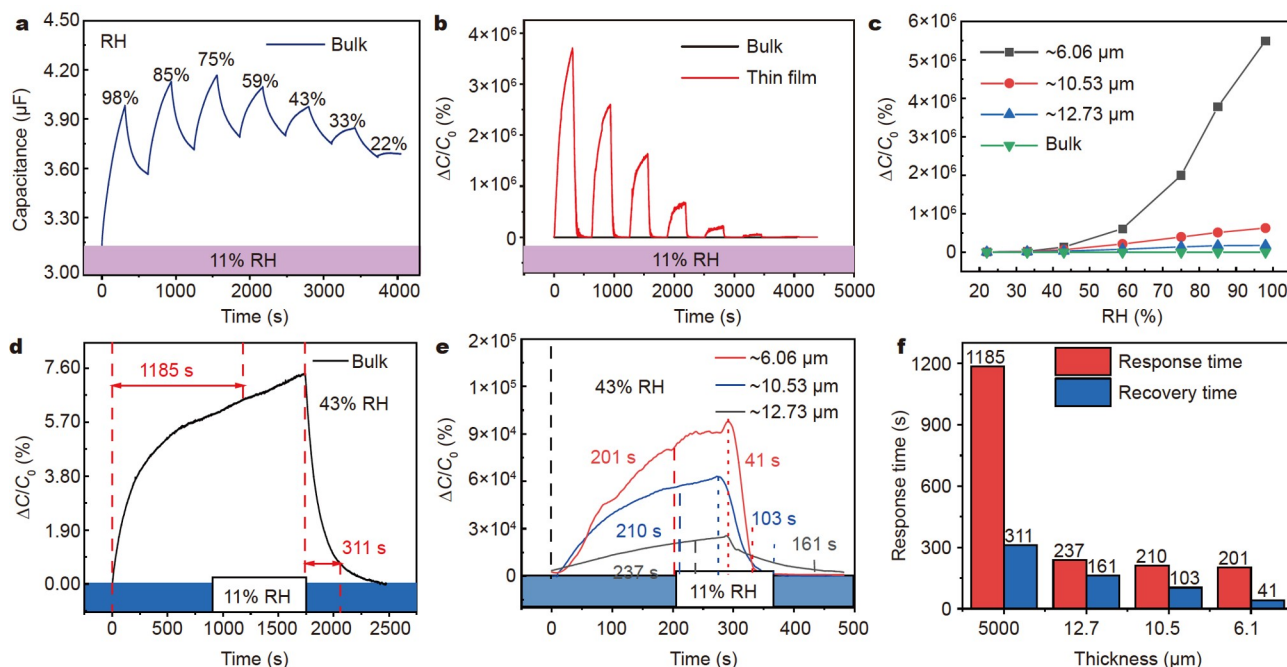

Figure 3 Impact of the thickness of the hydrogel layer on the humidity-sensing performance. (a) Dynamic capacitance variations of the bulk hydrogel under different RH ranges. (b) Dynamic capacitance responses of bulk and thin-film hydrogel sensors under different RH ranges. (c) RH-dependent variation of $\Delta C/C_0$ for the bulk and thin-film hydrogel sensors prepared with different thicknesses. (d, e) Response and recovery time analysis of the bulk and thin-film hydrogel sensors prepared with different thicknesses. (f) Comparison of the response and recovery times of the bulk and thin-film hydrogel sensors with different thicknesses.

Notably, the response and recovery speeds of hydrogel-based humidity sensors are also highly dependent on the thickness. The real-time response-recovery curves of hydrogel sensors with different thicknesses in the detection of 43% RH are shown in Fig. 3d, e. Rapid and reversible response and recovery processes are achieved using a thinner hydrogel film. Herein, the response and recovery times are defined as the time required to reach 90% of the total change in response, as shown in Fig. 3e. The bulk hydrogel sensor shows long response and recovery times of 1185 and 311 s, respectively. In comparison, the response times of the thin-film humidity sensors prepared at 500, 750, and 1000 r min^{-1} are reduced from 237 s to 210 and 201 s; meanwhile, the recovery time decreases from 161 s to 103 and 41 s, respectively. These results indicate that the reduction of the thickness of the hydrogel helps achieve the rapid adsorption and desorption of water molecules on its surface, which is consistent with the aforementioned contact angle measurement result.

Given that the humidity sensor needs to work under alternating current voltage when measuring the capacitance response (Fig. 4a), the influence of the test frequency on the performance of the thin-film sensor with the same hydrogel thickness of 6.06 μm was systematically investigated. As shown in Fig. 4b–d, the dynamic capacitance variations of the hydrogel film humidity sensor under different RH ranges were measured under different frequencies. Notably, the capacitance value of the sensor at 98% RH decreases from 100.8 nF to 66.6 and 21.2 nF with the increase in operating frequency from 200 Hz to 500 and 1000 Hz, respectively. Similarly, when the RH is as low as 11%, the capacitance values of the thin-film humidity sensor working at 200, 500, and 1000 Hz are 14.7, 9.4, and 7.1 pF, respectively (Fig. S6). Consequently, the response of the thin-film humidity sensor to 98% RH at 200 Hz is as high as 3,718,317%, whereas the responses at 500 and 1000 Hz are 908,836% and 388,601%,

respectively, indicating the remarkable dependence of the response on the operating frequency (Fig. 4e). As plotted in Fig. 4f, at the relatively high humidity (>59% RH), the sensitivity of the thin-film humidity sensor at 200 Hz is as high as 78,785.5%/% RH, which is 4.4 and 11.6 times that of 500 and 1000 Hz, respectively. Even at the low humidity (<59% RH), the sensitivity of the thin-film humidity sensor at 200 Hz reaches 18,484.7%/% RH, which is 3.8 and 5.4 times that of 500 and 1000 Hz, respectively. Presumably, the good sensitivity of the thin-film sensor at low operating frequencies can be attributed to the polarization of water molecules adsorbed on the hydrogel layer at low frequencies, which correspondingly increases the dielectric constant of the dielectric layer. Moreover, ions in hydrogel layers at low frequencies can keep up with the gradual change in the potential to form electrical double layers (EDLs) [63]. Therefore, 200 Hz is selected as the best working frequency in the experiment.

Herein, various representative stretchable humidity sensors based on different materials, such as reduced graphene oxide/polyurethane (RGO/PU) [57], WS$_2$ [58], acidified carbon nanotube/PU (ACNT/PU) [59], spandex covered yarns/polyaniline (SCY-PANI) [60], GO/PDMS [61], poly(sodium 4-styrenesulfonate)/poly(diallyldimethylammonium chloride)-agarose-PAM (PSS/PDAC-Agar-PAM) hydrogel [49], poly(vinyl alcohol) (PVA/KOH) [50], poly(acrylamide-*co*-sodium acrylate)/glycerol/Fe-citrate fiber (P(AAm-*co*-AA)/glycerol/Fe-citrate fiber) [64], and poly(3-dimethyl (methacryloyloxyethyl) ammonium propane sulfonate)/(1-ethyl-3-methylimidazolium ethyl sulfate)/poly(acrylic acid) (PDMAPS/IL/PAA) fiber/VHB elastomer [65] are summarized in Table 1, along with a comparison of their sensing performance. In stark contrast, our hydrogel thin-film humidity sensor exhibits an unprecedented sensitivity (78,785.5%/% RH), which is several orders of mag-
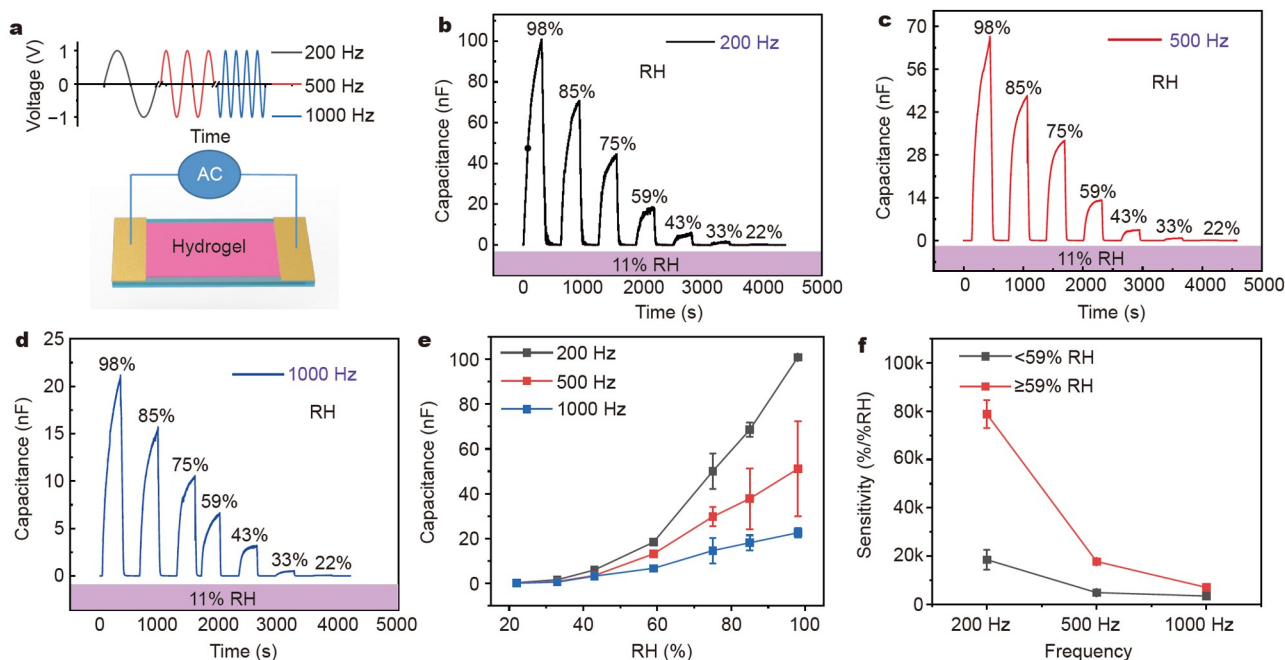

Figure 4 Relationship between operating frequency and sensing performance of the 6.06-μm-thick thin-film hydrogel sensor. (a) Schematic diagram of the thin-film sensor operating under different frequencies in the capacitance measurement mode. (b–d) Dynamic capacitance variations of the thin-film sensor in response to 22% to 98% RH when operating at 200, 500, and 1000 Hz. (e) RH-dependent variation of $\Delta C/C_0$ at the operating frequencies of 200, 500, and 1000 Hz. (f) Sensitivity of the thin-film humidity sensor *versus* frequency.

Table 1 Comparison of the sensing performance of stretchable humidity sensors based on different sensing materials

Sensing materials	Sensitivity (%/% RH) or response/% RH	Sensing range (% RH)	Response time/ recovery time (s)	Maximum strain	Transparency	Sensing mechanism
RGO/PU [57]	0.118%/% RH	10–70	3.5/7	60%	Yes	Resistance
WS$_2$ [58]	2357/90% RH	20–90	5/6	40%	Yes	Current
ACNT/PU [59]	28%/95% RH	11–95	NA/NA	100%	No	Resistance
SCY-PANI [60]	NA	20–90	116/NA	200%	No	Current
GO/PDMS [61]	NA	20–90	NA/NA	3%	Yes	Capacitance
PSS/PDAC-Agar-PAM hydrogel [49]	327 kΩ/13% RH, 23.9 kΩ/85% RH	13–85	3/94	400%	Yes	Resistance
PVA/KOH [50]	>70/(81.75% RH/10.89% RH)	6.4–93.5	0.4/2.6	383.6%	No	Current
P(AM-co-AA)/glycerol/Fe-citrate fiber [64]	47%/11% RH, 0%/90% RH	11–90	NA/NA	500%	Yes	Resistance
PDMAPS/PAA/IL fiber/VHB [65]	0.72 mV/% RH	5–70	NA/NA	1000%	Yes	Voltage
LiBr-PAM/carrageenan/PDMS [this work]	78,785.5%/% RH, 5,500,000%/98% RH	11–98	201/41	100%	Yes	Capacitance

nitude higher than those of reported bulky hydrogel sensors and miniature sensors based on low-dimensional materials, strongly proving the optimization effect of hydrogel miniaturization on the humidity-sensing performance of the hydrogel. Beyond that, this sensor also exhibits a wide detection range (11%–98% RH), fast response and recovery speeds (201/41 s), good stretchability (100%), and high transparency. Therefore, this sensor has significant advantages in practical wearable applications.

Notably, the PAM/carrageenan DN hydrogel is non-conductive. Meanwhile, the addition of KCl during the synthesis of the hydrogel not only promotes the formation of the double-helix carrageenan network but also endows the hydrogel with good ionic conductivity. Moreover, after the hydrogel is immersed in the LiBr solution, LiBr exists in the hydrogel in the form of ions, and the ionic conductivity of the hydrogel is further improved. Therefore, in addition to the capacitance response, the conductance responses of the hydrogel film humidity sensors were investigated in this work. As shown in Fig. S7, the capacitance and conductance of the thin-film humidity sensor have the same trend in response to different RH ranges. The conductance response of the thin-film humidity sensor to 98% RH has also reached 454,414%, which is only an order of magnitude smaller than the capacitance response. However, the conductance measurement mode provides another effective means to characterize the humidity-sensing performance for practical application, and understanding the sensing mechanism, which is complementary to the capacitance measurement mode, is helpful. In the conductance measurement mode, the increase in humidity leads to the migration of ions in the hydrogel layer, thereby increasing the conductance.

Given the significant influence of LiBr content on the ionic conductivity, its influence on the conductance change of the hydrogel film under different RH ranges was explored, and the amount of LiBr incorporated was controlled by the concentration of the LiBr solution. As expected, the results shown in Fig. S8 indicate that the conductivity of the hydrogel film sensor exposed to the same humidity increases as the concentration of the LiBr solution increases. Notably, the sensitivity of the LiBr-hydrogel film to humidity was negatively correlated with the concentration of the LiBr solution. As shown in Fig. S9, the measured conductance response of the hydrogel film sensors

immersed in 1 mol L^{-1} LiBr solution exhibits an exponential increase with the increase in humidity, whereas both film sensors immersed in 2 and 3 mol L^{-1} LiBr solutions exhibit a linear increase. As a result, the response of the hydrogel film to humidity decreases with the increase in LiBr, and when exposed to 98% RH, the response of the hydrogel film sensor immersed in 1 mol L^{-1} LiBr solution is 69.3 and 130.4 times higher than that of the film sensors treated with 2 and 3 mol L^{-1} LiBr, respectively. This finding can be attributed to the poor moisture desorption capability of the hydrogel under high LiBr content because of the excellent moisture-holding capability of LiBr. In detail, the relatively high conductivity of the hydrogel is still maintained at low humidity because of the high water content, which is inconducive to subsequent changes in conductivity upon the variation of environmental humidity, resulting in a reduced response. As shown in Fig. S8, comparing the recovery process (decrease in conductivity) of each sensor, the conductance of the hydrogel film sensor immersed in 1 mol L^{-1} LiBr solution decreases rapidly to the baseline, whereas the conductance of the other two sensors shows a smaller change and cannot reach a satisfactory stable baseline at the same time. This finding strongly confirms that the desorption of water molecules in the hydrogel becomes difficult as the amount of LiBr increases. Hence, there is a trade-off when considering the LiBr concentration introduced in the hydrogel film for the enhancement of sensitivity and conductivity. An appropriate LiBr concentration should be adopted to achieve balance in the performance.

To deeply understand the humidity-sensing mechanism of the hydrogel film, the complex impedance spectra of the hydrogel thin-film humidity sensors were measured under different RH ranges (Fig. 5a–c and Fig. S10). Furthermore, the relevant equivalent circuits were established based on complex impedance spectroscopy, as shown in the insets in Fig. 5a–c. Among them, R_1 and C_1 are the resistance and capacitance of the hydrogel film humidity sensor, respectively, and Z_w is the Warburg impedance, which is related to the ion diffusion process [66]. At 11% RH, the complex impedance spectrum is a complete semicircle. In this case, the equivalent circuit is composed of the resistance and capacitance of the hydrogel film in parallel. The ion diffusion effect inside the hydrogel film is not
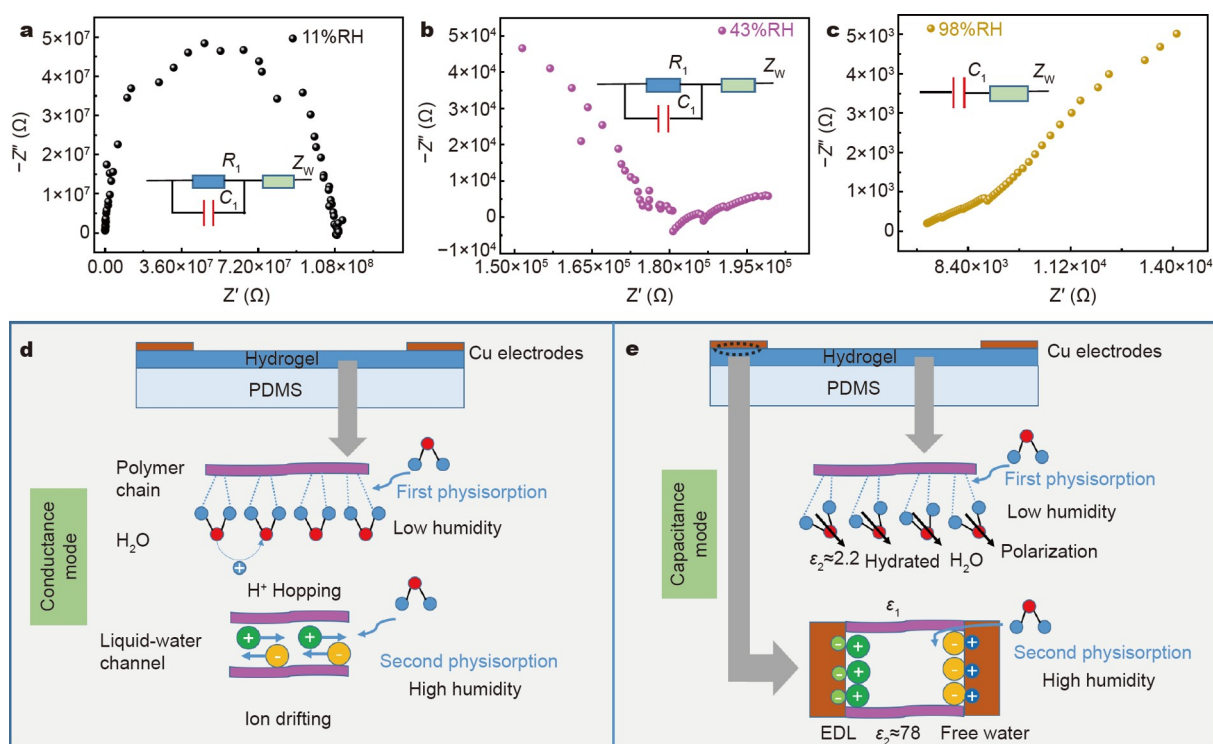
Figure 5 Investigation on the humidity-sensing mechanism. (a–c) Complex impedance plots of thin-film humidity sensors under different humidity levels. Insets are the equivalent circuits of the sensor at the corresponding RH. (d, e) Sensing mechanisms of the thin-film humidity sensor under conductance and capacitance measurement modes.

yet obvious; thus, the Warburg impedance is not generated. This finding indicates that, at low RH, water molecules in the hydrogel film are dispersed and discontinuous, which are only adsorbed on the surface of the hydrogel film and form hydrogen bonds with the hydrophilic groups (i.e., carboxyl, amino, hydroxyl, and sulfonate) on the polymer chains. As a result, the ions cannot migrate with the water as a medium, and the conductance mainly originates from proton hopping, resulting in a high resistance (Fig. 5d). Meanwhile, the capacitance of the hydrogel film is caused by the dielectric layer formed by the polarized water molecules and polymer chains under a low-frequency electric field (Fig. 5e) [67,68]. At 22% to 43% RH, the complex impedance spectrum becomes an incomplete semi-circle, and with the increase in humidity, an oblique short straight line gradually appears in the low-frequency region, corresponding to the generation of the Warburg impedance. Accordingly, the established equivalent circuit is composed of the resistance and capacitance of the hydrogel film and the Warburg impedance. In this humidity range, water molecules gradually penetrate the hydrogel film and reach the interior, and the hydrogel film resistance R_1 decreases. With the further increase in RH (i.e., 43%–59%), the semicircle gradually disappears and the oblique straight line gradually becomes longer, which indicates the continuous increase in the Warburg impedance, that is, the enhancement of ion diffusion in the hydrogel film. In this case, water molecules gradually form continuous water channels, and thus the ion mobility increases, leading to an increase in conductance (Fig. 5d). Meanwhile, more ions diffuse into the interface to form an EDL capacitance, resulting in a higher capacitance response (Fig. 5e). At 59%–98% RH, the complex impedance spectrum becomes an oblique straight line;

therefore, the impedance of the sensor is completely determined by the Warburg impedance. Herein, a large number of water molecules are adsorbed on the surface of the hydrogel film through physical adsorption and penetrate the hydrogel film, and thus the ion transport becomes more efficient, leading to a rapid increase in conductance. Moreover, because of the large dielectric constant of free water, the capacitance further increases.

Notably, compared with the bulk hydrogel sensor, in addition to the remarkably increased sensitivity and significantly reduced response/recovery time, excellent repeatability is exhibited by the thin-film hydrogel sensor, which is also an important performance indicator for determining whether the sensor can be used in practice. As shown in Fig. 6a–c and Fig. S11, the hydrogel film humidity sensor was exploited to detect 33%, 59%, and 98% RH for four to five consecutive cycles, and the response and recovery processes in each cycle were the same. The response error in the cycling test under different RH ranges is <1.8%, and particularly for the detection of low humidity (33%), the error is as small as 0.4%, reflecting the excellent repeatability. More importantly, the superb stretchability of both hydrogel and PDMS endows the corresponding hydrogel-based sensor with excellent deformability, which not only reduces the damage to the device caused by external forces but also increases the comfort level of wearable applications. In this work, because of the synergistic effect of the extension of the PAM network, the dynamic formation of hydrogen bonds, and the dissociation of the double-helix carrageenan structure in the PAM/carrageenan DN bulk hydrogel during stretching, it can be stretched to 1225% of its original length [7]. However, after thinning the hydrogel, the single-layer structure of the DN hydrogel film is
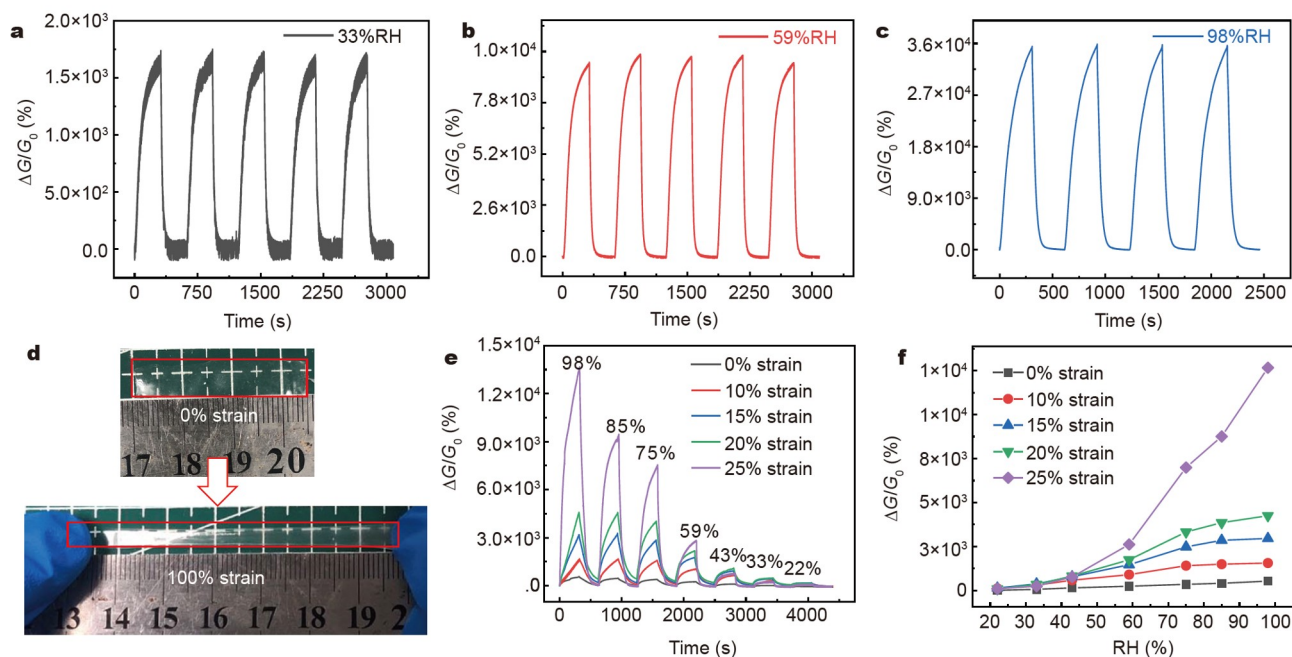
Figure 6 Repeatability and stretchability of the thin-film humidity sensor. Conductance responses of the sensor to the repeated switch of RH from 11% to 33% (a), 59% (b), and 98% (c). (d) Photographs of the same film sensor at 0% and 100% tensile strains. (e) Dynamic conductance responses of the sensor to 22% to 98% RH at 0%–25% tensile strains. (f) RH-dependent variation of $\Delta G/G_0$ at 0% to 25% tensile strains.

easier to shrink than spread out into a flat state. Therefore, the hydrogel film was selected to be prepared on a flexible PDMS substrate to form a double-layer structure, which can effectively maintain the flat morphology of the hydrogel film (Fig. 2b). As shown in Fig. 6d, the double layer PDMS-hydrogel hybrid exhibits a high stretchability of approximately 100% strain, which is higher than that of many non-hydrogel-based flexible humidity sensors and comparable to the maximum strain of human skin, meeting the stretchability requirement of electronic skin (Table 1) [58,61]. Because the LiBr-hydrogel film is soft (1.6 kPa) and thin, the mechanical properties of the hybrid depend on that of the PDMS substrate, such as Young's modulus (hybrid = 443.7 kPa, PDMS = 492.6 kPa) and maximum strain (Fig. S12). Furthermore, the effect of tensile deformation on the humidity response behavior of the hydrogel film sensor was systematically investigated, as shown in Fig. 6e, f. As the strain increases from 0% to 25%, the response of the sensor to 98% RH increases from 571% to 13,672%, and the sensitivity in the high humidity range (>59% RH) increases from 7.8%/% RH to 272.5%/% RH accordingly (Fig. S13). This positive correlation between humidity response and strain is consistent with the previously reported phenomenon, which can be attributed to the large exposure area of active adsorption sites and subsequent mass adsorption of water molecules after stretching [7,49]. In summary, the hydrogel film humidity sensor not only maintains the good stretchability of the bulk counterpart but also shows better sensing performance, particularly after stretching, making the sensing properties mechanically tunable.

Because high deformability, unprecedented responsiveness, wide detection range, excellent response/recovery speed, and repeatability are combined in the hydrogel film humidity sensor, it shows considerable potential for practical application in real life, such as for noncontact sensation and respiration monitor-

ing. Typically, the surface of the human skin contains moisture, which can correspondingly affect the RH near the surface of the hydrogel film when the finger approaches. As shown in Fig. 7a, in addition to simply detecting the proximity of the finger, our hydrogel film sensor can accurately determine the distance between the finger and the sensor interface through the conductance response value. As the finger gradually moves away from 5 to 9 mm from the sensor surface, the conductance response of the sensor correspondingly decreases from 645% to 262%, indicating a good resolution. According to this characteristic, this hydrogel film sensor can accurately monitor the subtle humidity fluctuation near the human skin surface based on the relationship between the humidity changes and the response signals, showing considerable potential for noncontact human-machine interaction. The noncontact sensation capacity helps prevent the transfer of some viruses between humans and machines, which is useful under the current global COVID-19 pandemic. Moreover, the exhaled air from the human body is a typical source of humidity, and the humidity changes under different respiratory frequencies vary. Although it takes a few minutes for the sensor to stabilize the signal, the sensor will be activated rapidly and reach a relatively high response in the first few seconds, which can be used for real-time humidity switch detection in practical sensing applications, such as breath monitoring (Fig. 7b). As shown in Fig. 7b and Fig. S14, the conductance changes of the hydrogel film sensor under different respiratory rates (i.e., 73, 16, and 12 breaths min^{-1}) are continuously monitored. The results show that the hydrogel film sensor placed under the nose can sensitively capture the subtle RH changes caused by breathing. Each peak in the dynamic response curve reflects a breath cycle, and the measured frequency is consistent with the actual human breath frequency. Furthermore, the peak intensity during a slow breath is higher
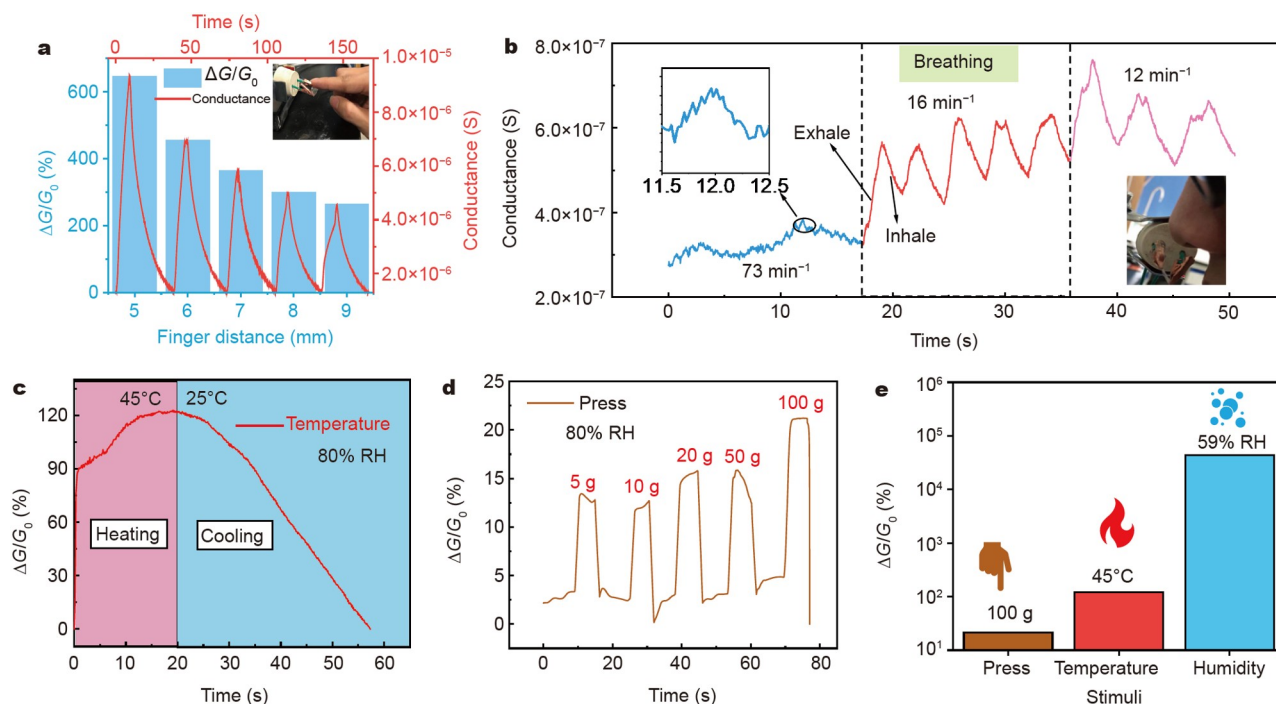
Figure 7 Practical applications of the hydrogel thin-film humidity sensor. (a) Dynamic conductance variation (right axis) and response ($\Delta G/G_0$; left axis) of the sensor to the approach of the finger with different distances between the finger and the surface of the sensor. (b) Real-time conductance variation of the sensor in response to human breath at a respiratory rate of 12–73 times min^{-1}. Dynamic conductance variations of the sensor to the switch of temperature between 25 and 45°C (c) and the loading of different pressures (d). (e) Comparison of the responses of the sensor to pressure (100 g), temperature (45°C), and humidity (59% RH).

than that during a fast breath because the larger amount of humid gas exhaled during the slow breath leads to the larger humidity difference and higher response. Inspired by these observations, these hydrogel thin-film sensors can be potentially applied in the wearable biomedical field to monitor the respiratory status of patients suffering from respiratory diseases, such as sleep dyspnea and obstructive pulmonary disease [69].

In addition to the humidity in the environment that can strongly affect the electrical properties of the hydrogel film sensor, other factors, such as temperature and pressure, may have similar effects. Therefore, the selectivity of the humidity sensor needs to be explored. To corroborate this finding, after the signal of the hydrogel thin-film sensor becomes stable, it is placed on a hot stage heated to 45°C, and its conductance response rapidly increases by 90% within 0.85 s and reaches a relatively stable value of 121% after 19 s (Fig. 7c). Furthermore, the influence of pressure on the electrical performance of the hydrogel thin-film sensor is explored by loading different weights on its surface. As shown in Fig. 7d, the pressure provided by the 5–100 g weights only produced 10% to 17% conductance responses, respectively, in the hydrogel thin-film sensor. Notably, these two sets of experiments were performed in an environment of approximately 80% RH. However, this sensor can produce a 43,335% conductance response to 59% RH, which is several orders of magnitude higher than the electrical responses caused by the common influence of temperature and pressure (Fig. 7e). Temperature only changes the speed of ion migration in the hydrogel, whereas pressure changes the thickness of the hydrogel. Neither of them causes a drastic change in the EDL, resulting in relatively low sensitivity. That is, both

temperature and pressure have only a slight effect on the accuracy of the hydrogel film humidity sensor, indicating good selectivity.

CONCLUSIONS

In summary, we successfully prepared hydrogel thin films with different thicknesses through spin-coating technology, and the corresponding hydrogel film humidity sensors were constructed. The comparative study shows that the responses of these sensors show a remarkable thickness dependence, and an unprecedented improvement in sensing performance is achieved because of the miniaturization effect of the hydrogel. Benefiting from the large exposure area of chemical bonds after the thinning of the hydrogel, the thinnest (i.e., 6.06 μm thick) hydrogel-film-based humidity sensor exhibits sensitivity as high as 78,785.5%/% RH, and its response to 98% RH is 203,703 times higher than that of the bulk hydrogel. Meanwhile, this sensor exhibits a wide detection range, fast response/recovery speed, good stretchability, high transparency, repeatability, and selectivity, showing significant performance advantages compared with traditional humidity sensors. The humidity-sensing mechanism of ion-conducting hydrogel is also elucidated by the complex impedance spectra. Various proof-of-concept studies show that this ultrasensitive humidity sensor can potentially be used in real-time physiological monitoring and noncontact sensing triggered by human humidity. Different from previously reported hydrogel-based sensors focusing on materials innovation or function optimization, the paradigm of the high-performance, stretchable, and transparent thin-film sensor is considered to be a universal and high-efficiency strategy for future fabrication of

miniaturized and advanced hydrogel-based electronics used in biosensing, wearable devices, and health monitoring.

1 Azevedo S, Costa AMS, Andersen A, et al. Bioinspired ultratough hydrogel with fast recovery, self-healing, injectability and cytocompatibility. Adv Mater, 2017, 29: 1700759

2 Mo F, Chen Z, Liang G, et al. Zwitterionic sulfobetaine hydrogel electrolyte building separated positive/negative ion migration channels for aqueous Zn-MnO_2 batteries with superior rate capabilities. Adv Energy Mater, 2020, 10: 2000035

3 Lee J, Tan MWM, Parida K, et al. Water-processable, stretchable, self-healable, thermally stable, and transparent ionic conductors for actuators and sensors. Adv Mater, 2020, 32: 1906679

4 Farid T, Rafiq MI, Ali A, et al. Transforming wood as next-generation structural and functional materials for a sustainable future. EcoMat, 2022, 4: e12154

5 Ding Q, Wu Z, Tao K, et al. Environment tolerant, adaptable and stretchable organohydrogels: Preparation, optimization, and applications. Mater Horiz, 2022, doi: 10.1039/D1MH01871J

6 Tao K, Chen Z, Yu J, et al. Ultra-sensitive, deformable, and transparent triboelectric tactile sensor based on micro-pyramid patterned ionic hydrogel for interactive human-machine interfaces. Adv Sci, 2022, 9: 2104168

7 Wu J, Wu Z, Xu H, et al. An intrinsically stretchable humidity sensor based on anti-drying, self-healing and transparent organohydrogels. Mater Horiz, 2019, 6: 595–603

8 Wu J, Wu Z, Han S, et al. Extremely deformable, transparent, and high-performance gas sensor based on ionic conductive hydrogel. ACS Appl Mater Interfaces, 2018, 11: 2364–2373

9 Ge G, Lu Y, Qu X, et al. Muscle-inspired self-healing hydrogels for strain and temperature sensor. ACS Nano, 2019, 14: 218–228

10 Wu J, Han S, Yang T, et al. Highly stretchable and transparent thermistor based on self-healing double network hydrogel. ACS Appl Mater Interfaces, 2018, 10: 19097–19105

11 Deng Z, Hu T, Lei Q, et al. Stimuli-responsive conductive nanocomposite hydrogels with high stretchability, self-healing, adhesiveness, and 3D printability for human motion sensing. ACS Appl Mater Interfaces, 2019, 11: 6796–6808

12 Deng Z, Wang H, Ma PX, et al. Self-healing conductive hydrogels: Preparation, properties and applications. Nanoscale, 2020, 12: 1224–1246

13 Deng Z, Yu R, Guo B. Stimuli-responsive conductive hydrogels: Design, properties, and applications. Mater Chem Front, 2021, 5: 2092–2123

14 Liang Y, Wu Z, Wei Y, et al. Self-healing, self-adhesive and stable organohydrogel-based stretchable oxygen sensor with high performance at room temperature. Nano-Micro Lett, 2022, 14: 52

15 Ding H, Wu Z, Wang H, et al. An ultrastretchable, high-performance, and crosstalk-free proximity and pressure bimodal sensor based on ionic hydrogel fibers for human-machine interfaces. Mater Horiz, 2022, doi: 10.1039/D2MH00281G

16 Wei Y, Wang H, Ding Q, et al. Hydrogel- and organohydrogel-based stretchable, ultrasensitive, transparent, room-temperature and real-time NO_2 sensors and the mechanism. Mater Horiz, 2022, doi: 10.1039/D2MH00284A

17 Zhang C, Wu B, Zhou Y, et al. Mussel-inspired hydrogels: From design principles to promising applications. Chem Soc Rev, 2020, 49: 3605–3637

18 Yang C, Suo Z. Hydrogel ionotronics. Nat Rev Mater, 2018, 3: 125–142

19 Le HH, Tran VT, Mredha MTI, et al. Thin-film hydrogels with superior stiffness, strength, and stretchability. Extreme Mech Lett, 2020, 37: 100720

20 Wu Z, Yang X, Wu J. Conductive hydrogel- and organohydrogel-based stretchable sensors. ACS Appl Mater Interfaces, 2021, 13: 2128–2144

21 Mo F, Liang G, Wang D, et al. Biomimetic organohydrogel electrolytes for high-environmental adaptive energy storage devices. EcoMat, 2019, 1: e12008

22 Wu S, Alsaid Y, Yao B, et al. Rapid and scalable fabrication of ultra-stretchable, anti-freezing conductive gels by cononsolvency effect. EcoMat, 2021, 3: e12085

23 Lu L, Jiang C, Hu G, et al. Flexible noncontact sensing for human-machine interaction. Adv Mater, 2021, 33: 2100218

24 Jeong W, Song J, Bae J, et al. Breathable nanomesh humidity sensor for real-time skin humidity monitoring. ACS Appl Mater Interfaces, 2019, 11: 44758–44763

25 Massaroni C, Nicolò A, Schena E, et al. Remote respiratory monitoring in the time of COVID-19. Front Physiol, 2020, 11: 635

26 Zhu P, Liu Y, Fang Z, et al. Flexible and highly sensitive humidity sensor based on cellulose nanofibers and carbon nanotube composite film. Langmuir, 2019, 35: 4834–4842

27 Li B, Xiao G, Liu F, et al. A flexible humidity sensor based on silk fabrics for human respiration monitoring. J Mater Chem C, 2018, 6: 4549–4554

28 Lan L, Le X, Dong H, et al. One-step and large-scale fabrication of flexible and wearable humidity sensor based on laser-induced graphene for real-time tracking of plant transpiration at bio-interface. Biosens Bioelectron, 2020, 165: 112360

29 Park R, Kim H, Lone S, et al. One-step laser patterned highly uniform reduced graphene oxide thin films for circuit-enabled tattoo and flexible humidity sensor application. Sensors, 2018, 18: 1857

30 Songkeaw P, Onlaor K, Thiwawong T, et al. Transparent and flexible humidity sensor based on graphene oxide thin films prepared by electrostatic spray deposition technique. J Mater Sci-Mater Electron, 2020, 31: 12206–12215

31 Zhang X, Maddipatla D, Bose AK, et al. Printed carbon nanotubes-based flexible resistive humidity sensor. IEEE Sens J, 2020, 20: 12592–12601

32 Zhou C, Zhang X, Tang N, et al. Rapid response flexible humidity sensor for respiration monitoring using nano-confined strategy. Nanotechnology, 2020, 31: 125302

33 Wu J, Wu Z, Ding H, et al. Multifunctional and high-sensitive sensor capable of detecting humidity, temperature, and flow stimuli using an integrated microheater. ACS Appl Mater Interfaces, 2019, 11: 43383–43392

34 Wu J, Sun YM, Wu Z, et al. Carbon nanocoil-based fast-response and flexible humidity sensor for multifunctional applications. ACS Appl Mater Interfaces, 2019, 11: 4242–4251

35 Cai J, Lv C, Aoyagi E, et al. Laser direct writing of a high-performance all-graphene humidity sensor working in a novel sensing mode for portable electronics. ACS Appl Mater Interfaces, 2018, 10: 23987–23996

36 Hajian S, Zhang X, Maddipatla D, et al. Development of a fluorinated graphene-based flexible humidity sensor. In: 2019 IEEE International Conference on Flexible and Printable Sensors and Systems (FLEPS), Glasgow, 2019, 1–3

37 Zhang D, Zong X, Wu Z, et al. Hierarchical self-assembled SnS_2 nanoflower/Zn_2SnO_4 hollow sphere nanohybrid for humidity-sensing applications. ACS Appl Mater Interfaces, 2018, 10: 32631–32639

38 Guo J, Wen R, Liu Y, et al. Piezotronic effect enhanced flexible humidity sensing of monolayer MoS_2. ACS Appl Mater Interfaces, 2018, 10: 8110–8116

39 Jenjeti RN, Kumar R, Sampath S. Two-dimensional, few-layer $NiPS_3$ for flexible humidity sensor with high selectivity. J Mater Chem A, 2019, 7: 14545–14551

40 Duy LT, Baek JY, Mun YJ, et al. Patternable production of $SrTiO_3$ nanoparticles using 1-W laser directly on flexible humidity sensor platform based on ITO/$SrTiO_3$/CNT. J Mater Sci Tech, 2021, 71: 186–194

41 Feng Y, Gong S, Du E, et al. TaS_2 nanosheet-based ultrafast response and flexible humidity sensor for multifunctional applications. J Mater Chem C, 2019, 7: 9284–9292

42 Jeong H, Noh Y, Lee D. Highly stable and sensitive resistive flexible humidity sensors by means of roll-to-roll printed electrodes and flower-like TiO_2 nanostructures. Ceramics Int, 2019, 45: 985–992

43 Kim H, Park S, Park Y, et al. Fabrication of a semi-transparent flexible humidity sensor using kinetically sprayed cupric oxide film. Sens Actuat B-Chem, 2018, 274: 331–337

44 Zhou G, Byun JH, Oh Y, *et al.* Highly sensitive wearable textile-based humidity sensor made of high-strength, single-walled carbon nanotube/poly(vinyl alcohol) filaments. ACS Appl Mater Interfaces, 2017, 9: 4788–4797

45 Wang Y, Zhang L, Zhou J, *et al.* Flexible and transparent cellulose-based ionic film as a humidity sensor. ACS Appl Mater Interfaces, 2020, 12: 7631–7638

46 Zhang D, Jiang C, Sun Y, *et al.* Layer-by-layer self-assembly of tricobalt tetraoxide-polymer nanocomposite toward high-performance humidity-sensing. J Alloys Compd, 2017, 711: 652–658

47 Zhang D, Zong X, Wu Z. Fabrication of tin disulfide/graphene oxide nanoflower on flexible substrate for ultrasensitive humidity sensing with ultralow hysteresis and good reversibility. Sens Actuat B-Chem, 2019, 287: 398–407

48 Qi P, Zhang T, Shao J, *et al.* A QCM humidity sensor constructed by graphene quantum dots and chitosan composites. Sens Actuat A-Phys, 2019, 287: 93–101

49 Ying B, Wu Q, Li J, *et al.* An ambient-stable and stretchable ionic skin with multimodal sensation. Mater Horiz, 2020, 7: 477–488

50 Li T, Li L, Sun H, *et al.* Porous ionic membrane based flexible humidity sensor and its multifunctional applications. Adv Sci, 2017, 4: 1600404

51 Lim C, Hong YJ, Jung J, *et al.* Tissue-like skin-device interface for wearable bioelectronics by using ultrasoft, mass-permeable, and low-impedance hydrogels. Sci Adv, 2021, 7: eabd3716

52 Chen X, He M, Zhang X, *et al.* Metal-free and stretchable conductive hydrogels for high transparent conductive film and flexible strain sensor with high sensitivity. Macromol Chem Phys, 2020, 221: 2000054

53 Wu Z, Ding H, Tao K, *et al.* Ultrasensitive, stretchable, and fast-response temperature sensors based on hydrogel films for wearable applications. ACS Appl Mater Interfaces, 2021, 13: 21854–21864

54 Buchberger A, Peterka S, Coclite AM, *et al.* Fast optical humidity sensor based on hydrogel thin film expansion for harsh environment. Sensors, 2019, 19: 999

55 Huang Y, Zhang X, Ma Z, *et al.* Hydrogen-bond relaxation dynamics: Resolving mysteries of water ice. Coord Chem Rev, 2015, 285: 109–165

56 Wu Z, Shi W, Ding H, *et al.* Ultrastable, stretchable, highly conductive and transparent hydrogels enabled by salt-percolation for high-performance temperature and strain sensing. J Mater Chem C, 2021, 9: 13668–13679

57 Trung TQ, Duy LT, Ramasundaram S, *et al.* Transparent, stretchable, and rapid-response humidity sensor for body-attachable wearable electronics. Nano Res, 2017, 10: 2021–2033

58 Guo H, Lan C, Zhou Z, *et al.* Transparent, flexible, and stretchable WS₂ based humidity sensors for electronic skin. Nanoscale, 2017, 9: 6246–6253

59 Huang X, Li B, Wang L, *et al.* Superhydrophilic, underwater super-oleophobic, and highly stretchable humidity and chemical vapor sensors for human breath detection. ACS Appl Mater Interfaces, 2019, 11: 24533–24543

60 Guo YN, Gao ZY, Wang XX, *et al.* A highly stretchable humidity sensor based on spandex covered yarns and nanostructured polyaniline. RSC Adv, 2018, 8: 1078–1082

61 Ho DH, Sun Q, Kim SY, *et al.* Stretchable and multimodal all graphene electronic skin. Adv Mater, 2016, 28: 2601–2608

62 Li Y, Pham JQ, Johnston KP, *et al.* Contact angle of water on polystyrene thin films: Effects of CO₂ environment and film thickness. Langmuir, 2007, 23: 9785–9793

63 Islam T, Ur Rahman MZ. Investigation of the electrical characteristics on measurement frequency of a thin-film ceramic humidity sensor. IEEE Trans Instrum Meas, 2016, 65: 694–702

64 Ju M, Wu B, Sun S, *et al.* Redox-active iron-citrate complex regulated robust coating-free hydrogel microfiber net with high environmental tolerance and sensitivity. Adv Funct Mater, 2020, 30: 1910387

65 Lei Z, Wu P. A highly transparent and ultra-stretchable conductor with stable conductivity during large deformation. Nat Commun, 2019, 10: 3429

66 Huang J. Diffusion impedance of electroactive materials, electrolytic solutions and porous electrodes: Warburg impedance and beyond. Electrochim Acta, 2018, 281: 170–188

67 Bi H, Yin K, Xie X, *et al.* Ultrahigh humidity sensitivity of graphene oxide. Sci Rep, 2013, 3: 2714

68 Li N, Chen X, Chen X, *et al.* Ultrahigh humidity sensitivity of graphene oxide combined with Ag nanoparticles. RSC Adv, 2017, 7: 45988–45996

69 Zammit C, Liddicoat H, Moonsie I, *et al.* Obesity and respiratory diseases. Int J Gen Med, 2010, 3: 335

Author contributions Wu J, Wu Z, Ding Q, and Li Z designed the sensors, analyzed the results, and wrote the paper; Wu Z drafted the manuscript; Zhou Z, Luo L, Tao K, and Xie X contributed to the discussion of the results; Wu J revised the paper and supervised the project. All authors contributed to the general discussion.

Conflict of interest The authors declare that they have no conflict of interest.

Supplementary information Supporting data are available in the online version of the paper.

Jin Wu received his PhD degree from Nanyang Technological University in 2014. After obtaining his PhD degree in 2014, he continued working in the SMART program at Nanyang Technological University as a postdoctoral research fellow. Since 2017, he has been an associate professor at the School of Electronics and Information Technology, Sun Yat-sen University. His research interest includes hydrogel-based sensors, and flexible and stretchable electronics.

基于离子导电双网络水凝胶薄膜的超灵敏、可拉伸、透明湿度传感器

吴子轩[1†], 丁琼玲[1†], 李振毅[1†], 周子敬[1], 罗璐琪[1], 陶凯[2], 谢曦[1], 吴进[1*]

摘要 本工作中, 我们在可拉伸的弹性基底上集成了厚度可控的可拉伸、透明的双网络导电水凝胶薄膜, 它具有很好的环境稳定性以及对湿度极高的响应灵敏度(78,785.5%/% RH). 与块体水凝胶相比, 基于水凝胶薄膜的湿度传感器对98% RH的响应提高了2×10⁵倍, 另外, 响应和恢复速度分别提高了5.9倍和7.6倍. 这得益于水凝胶薄膜超高的比表面积, 丰富的活性吸附位点以及短的扩散距离. 研究发现水凝胶的湿度传感性能具有显著的厚度依赖性. 系统的湿敏机理研究表明: 水分子的吸附提高了水凝胶的离子迁移率和介电常数, 并且形成了双电层, 从而实现了对湿度的超高电学响应. 此外, 该传感器能够实现非接触式人机交互以及实时地检测人体呼吸. 这项工作作为实现器件性能的突破以及推动水凝胶基集成微电子技术的发展提供了新策略.